Received: Added at production | Revised: Added at production | Accepted: Added at production

DOI: xxx/xxxx

ORIGINAL ARTICLE

LLC Resonant Converter Based on PFM and Secondary-Side Short-Circuit Control for On-Board Charger

Yu Tang*[1] | Baolin Zhao[1] | Zhe Shi[1] | Lin Jiang[2] | Yun Zhang[3]

[1]State Key Laboratory of Reliability and Intelligence of Electrical Equipment, Hebei University of Technology, Tianjin, China
[2]Department of Electrical Engineering and Electronics, University of Liverpool, Liverpool, U.K.
[3]School of Electrical and Information Engineering, Tianjin University, Tianjin, China

Correspondence
Yu Tang, State Key Laboratory of Reliability and Intelligence of Electrical Equipment, School of Electrical Engineering, Hebei University of Technology, Tianjin 300130, China. Email: ty8025@hotmail.com

Abstract

Commonly used lithium-ion battery on-board charger (OBC) for electric vehicles (EVs) needs a wide output voltage range, but the traditional *LLC* converter is hard to meet the need under the condition of high efficiency and high power density. In this paper, a resonant converter with hybrid modulation is proposed. The converter has a relatively simple topology and control method. Compared with the traditional *LLC* topology, only two diodes are replaced by MOSFETs on the secondary side of the transformer, and no auxiliary components are added. The primary-side switches adopt pulse frequency modulation (PFM) and the secondary-side switches adopt short-circuit control in the proposed converter, which can realize a wide output voltage range, in a narrow switching frequency range with excellent soft-switching performance. The proposed converter can effectively reduce the resonant current and the volume of transformer core, and achieve energy delivery with high power density and high efficiency. The operation principles, voltage gain, and soft-switching conditions of the converter are analyzed in this paper. Finally, a 3.3 kW SiC-based prototype with 400V input and 250V-430V output is built to verify the feasibility and validity of the proposed converter.

KEYWORDS:
On-board charger (OBC), electric vehicle (EV), *LLC* resonant converter, hybrid modulation, wide output range.

1 | INTRODUCTION

In recent years, electric vehicles (EVs) have been favored by people due to their potential to alleviate fossil fuel crisis and increase energy sustainability. With the increasing capacity of the power battery packs of EVs on the market, the research on on-board charger (OBC) has gradually become a hot spot all over the world [1,2,3,4]. Lithium battery has become the most widely used battery for EVs globally because of its high energy density, good safety, long cycle life, and low cost [5]. The CC-CV (constant current-constant voltage) two-stage charging method is the primary way to charge lithium battery at present. However, the CC-CV charging method makes the battery pack charging process with a wide voltage range. At present, the output voltage range of OBC is approximately 200V-450V. Therefore, it is necessary to design a DC-DC converter with a wide output voltage range and high efficiency. *LLC* converter has been widely concerned by scholars because it is capable of zero-voltage switching (ZVS) on the primary side and zero-current switching (ZCS) on the secondary side under certain conditions with low electromagnetic interference and high power density [6,7,8].

However, to achieve a wide output range, the circuit parameters of the *LLC* converter need to be adjusted, or the converter needs to operate in a wide frequency range. On the one hand, if the circuit parameters are adjusted, the ratio of the magnetizing inductor L_m to the resonant inductor L_r needs to be reduced. When L_m decreases, the magnetizing current will increase, resulting in higher losses. While increasing L_r will lead to an increase in converter size, thus reducing the power density. On the other hand, if the converter works in a wide frequency range, the switching frequency will be far away from the resonant frequency, which will cause a higher circulating current and thus increase the losses[9]. And as the operating range less than the resonant frequency increases, the volume of the transformer will also expand. In addition, when the input voltage is constant, as the output voltage gets higher, the switching frequency of the *LLC* converter decreases with the increase of magnetizing current. This increases the maximum magnetic flux density of the transformer and requires a larger magnetic core size when designing the transformer, which leads to a reduction in the power density of the converter.

Therefore, the traditional *LLC* converter cannot perfectly meet the needs of wide output voltage applications. Recently, a large number of scholars have conducted a series of researches around widening the output range and improving efficiency.

Some methods attempting to adjust the voltage by changing the modulation strategies are proposed in literature.[10,11,12,13,14,15] In literature,[10,11,12,13] the burst mode strategy is employed in the converter to improve the performance at light load and the efficiency of the converter. However, this not only increases the control complexity, but also brings low-frequency output voltage ripple and EMI problems to the system. In literature,[14] the asymmetric PWM (APWM) control is used to expand the voltage regulation range. However, this results in a DC bias in the magnetizing current flowing through transformer. In literature,[15] Phase-shift modulation (PSM) of the primary switching network is adopted to reduce the switching frequency of the *LLC* converter. Hence, the core loss of the transformer can be reduced, and a higher power density can be achieved. However, excessive turn-off current of the primary side increases losses under heavy load condition. Some researchers in literature[16,17,18,19] focus on adding components in the primary side to increase the gain. In literature,[16] by adding a notch *LC* filter to the *LLC* tank, the converter can be soft-switched over the whole output voltage range with soft startup and over-current protection. However, analysis of the topology is complex and efficiency decreases at high output voltage. The authors in literature,[17] combined Sepic and half-bridge *LLC* converter in the primary side to achieve high efficiency in a wide voltage range. Nevertheless, bulky inductors and capacitors are required in the converter, which reduces the power density. In literature,[18] an *LLC* resonant converter with three operating modes is proposed to achieve higher efficiency and power density over a wide voltage range by adding a resonant inductor and transformer in the primary side. However, the converter needs two identical transformers, and the leakage inductance deviation of the transformers will cause current bias. In literature,[19] the proposed topology uses three resonant tanks to regulate the output voltage. The converter can operate in full-bridge mode and half-bridge mode with ZVS. However, adding extra components increase extra losses and the system complexity.

In literature,[20,21] the secondary-side switching networks are reconfigured to achieve a wide output voltage range. In literature,[20] a variable structure rectifier consisting of a switched capacitor, two active switches, two diodes, and two output capacitors is proposed to expand the output voltage range by PWM control. Although these structures can extend the output voltage range, the introduction of additional components will bring more conduction losses and costs. In literature,[21] two rectifying diodes are replaced with GaN MOSFETs on the secondary side to realize a wide output voltage range in a narrow switching frequency by specific modulation. However, the control scheme proposed in this paper needs to detect the drain-source voltage of the secondary-side switches to probe the zero-crossing time of resonant current, which increases the complexity of system. Additionally, the long conduction time of the body diodes of the secondary-side MOSFETs results in high conduction losses.

In this article, a resonant converter with hybrid modulation is proposed, which adopts pulse frequency modulation (PFM) on the primary side and short-circuit control on the secondary side. Compared with the traditional *LLC* converter, only two rectifier diodes are replaced by MOSFETs on the secondary side, and no auxiliary components are added. The proposed converter is able to achieve a wide output voltage range with good soft-switching performance in a narrow switching frequency range by a relatively simple control method. As a result, the size of the transformer core and the conduction losses are reduced, making it more competitive for OBC applications. Finally, a 3.3 kW prototype with 400V input and 250V-430V output has been built using SiC switching devices to verify the theoretical analysis the effectiveness of the converter.

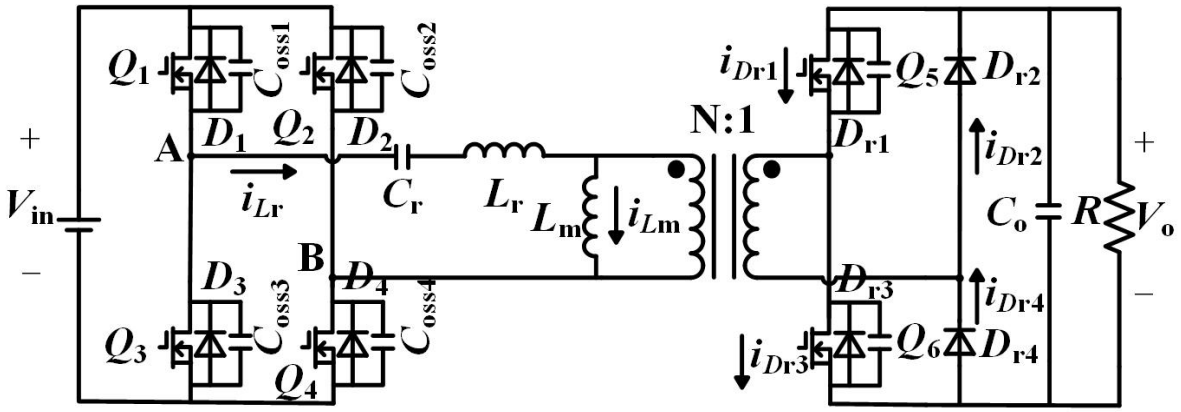

FIGURE 1 Proposed resonant converter with hybrid modulation.

2 | PROPOSED CONVERTER AND OPERATIONAL PRINCIPLE

The schematic of the proposed resonant converter is illustrated in Fig. 1. In terms of circuit structure, one switching leg of the full-bridge rectifier diodes is substituted by MOSFETs, which is the only change from a standard *LLC* resonant converter. Depending on the output voltage gain, the converter operates in PFM control mode or short-circuit control mode.

The short-circuit control mode is adopted when the voltage gain is higher than 1. At this time, the switching frequency is fixed at the resonant frequency f_r, and the driving signals for Q_5 and Q_6 of the secondary side lag behind the driving signals of the primary side. The lag time is DT, where D ($0 < D < 1$) represents the short-circuit duty cycle, and T represents the switching period. By short-circuiting the secondary side, the energy stored in the resonant inductor L_r is increased to boost the output voltage. Fig. 2 shows the waveforms of key parameters in short-circuit control mode.

When the converter operates in short-circuit control mode during steady-state operation, the working process can be separated into ten stages in a single switching period. Due to the symmetry of the operation, only five stages of the first half period are discussed here. The equivalent circuits of the first five stages over a half switching period are illustrated in Fig. 3.

Mode I [t_0-t_1]. At t_0, i_{Lr} equals to i_{Lm}, the resonant current i_{Lr} is negative, which discharges the parallel capacitors C_{oss1} and C_{oss4} of the switches Q_1 and Q_4 while charging parallel capacitors C_{oss2} and C_{oss3} of the switches Q_2 and Q_3, providing the conditions for Q_1 and Q_4 to achieve ZVS. The voltage flowing through the transformer is positive during this stage, which enables the conductions of Q_6 and D_{r4}. Hence, the voltage on L_m is clamped to zero by short-circuiting the secondary side. No energy is transmitted from the primary side to the load in this time interval, and the load voltage is maintained by the output capacitor C_o.

Mode II [t_1-t_2]. Q_1 and Q_4 achieve ZVS at t_1. Since i_{Lm} is larger than i_{Lr} in this stage, the short circuit state on the secondary side continues with the conductions of Q_6 and D_{r4}. The resonant current i_{Lr} rises rapidly with the resonance between L_r and C_r. As the voltage across L_m is clamped to zero, i_{Lm} remains constant. At t_2, Q_6 turns off, which marks the end of this mode. The electronic equations in this stage can be expressed as follows:

$$\begin{cases} C_r \frac{dv_{Cr}}{dt} = i_{Lr} \\ V_{in} - v_{Cr} = L_r \frac{di_{Lr}}{dt} \end{cases}, \begin{cases} v_{Cr}(t_1) = V_{Cr0} \\ i_{Lr}(t_1) = I_{Lr0} \end{cases} \tag{1}$$

v_{Cr} and i_{Lr} can be obtained as:

$$\begin{cases} v_{Cr} = V_{in} + (V_{Cr0} - V_{in}) \cos w_r(t - t_1) + I_{Lr0} Z_r \sin w_r(t - t_1) \\ i_{Lr} = I_{Lr0} \cos w_r(t - t_1) + \frac{V_{in} - V_{Cr0}}{Z_r} \sin w_r(t - t_1) \end{cases} \tag{2}$$

where $w_r = 1/\sqrt{L_r C_r}$ is the angular resonant frequency, $Z_r = \sqrt{L_r/C_r}$ is the characteristic impedance of the resonant tank, and the magnetizing current can be expressed as $i_{Lm} = i_{Lr}(t_1) = I_{Lr0}$.

Mode III [t_2-t_3]. The voltage flowing through the transformer remains positive after Q_6 turns off at t_2. Meanwhile, the primary energy is delivered to the load through the body diode of Q_5 and the diode D_{r4}. The voltage on L_m is clamped to nV_o, causing

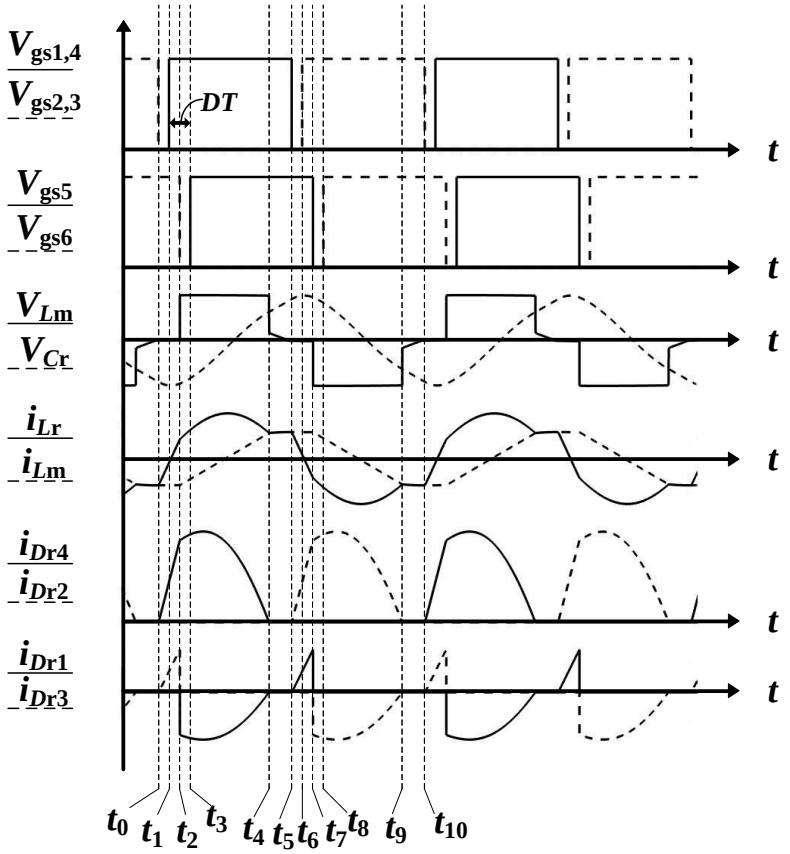

FIGURE 2 Key waveforms of the short-circuit control mode.

the decline of the magnetizing current. Besides, as the body diode of Q_5 is turned on, the voltage across the parallel capacitors of Q_5 is zero, which provides the condition for the realization of ZVS.

Mode IV [t_3-t_4]. Q_5 achieves ZVS at t_3. The working state in this mode is similar to the conventional *LLC* resonant converter with frequency modulation. L_r continues to resonant with C_r with the voltage $(V_{in} - nV_o)$ applied to the resonant tank consisting of L_r and C_r. This mode lasts until the moment t_4 when i_{Lm} equals i_{Lr}. The electronic equations in [t_2-t_4] can be expressed as follows:

$$\begin{cases} C_r \frac{dv_{Cr}}{dt} = i_{Lr} \\ V_{in} - v_{Cr} - V_o = L_r \frac{di_{Lr}}{dt} \end{cases}, \begin{cases} v_{Cr}(t_2) = V_{Cr1} \\ i_{Lr}(t_2) = I_{Lr1} \end{cases} \tag{3}$$

v_{Cr} and i_{Lr} can be obtained as:

$$\begin{cases} v_{Cr} = V_{in} - nV_o + (V_{Cr1} - V_{in} + nV_o)\cos w_r(t - t_2) + I_{Lr1} Z_r \sin w_r(t - t_2) \\ i_{Lr} = I_{Lr1}\cos w_r(t - t_2) + \frac{V_{in} - nV_o - V_{Cr1}}{Z_r} \sin w_r(t - t_2) \end{cases} \tag{4}$$

i_{Lm} can be expressed as:

$$i_{Lm} = I_{Lr0} + \frac{nV_o}{L_m}(t - t_2) \tag{5}$$

Mode V [t_4-t_5]. i_{Lm} equals to i_{Lr} at t_4. The secondary current naturally drops to zero. Thus, the secondary diodes achieve ZCS without reverse recovery. L_m begins to resonate with L_r and C_r. Since $(L_m + L_r)$ is much larger than L_r, the resonant current i_{Lr} can be approximated as a constant. Mode V ends when Q_1 and Q_4 turn OFF at t_5. The state equations in this mode are shown as:

$$\begin{cases} C_r \frac{dv_{Cr}}{dt} = i_{Lr} \\ V_{in} - v_{Cr} = (L_r + L_m)\frac{di_{Lr}}{dt} \end{cases}, \begin{cases} v_{Cr}(t_4) = V_{Cr2} \\ i_{Lr}(t_4) = I_{Lr2} \end{cases} \tag{6}$$

We can approximately assume:

$$\begin{cases} i_{Lr} = I_{Lr2} \\ v_{Cr} = V_{Cr2} + \frac{I_{Lr2}}{C_r}(t - t_4) \end{cases} \tag{7}$$

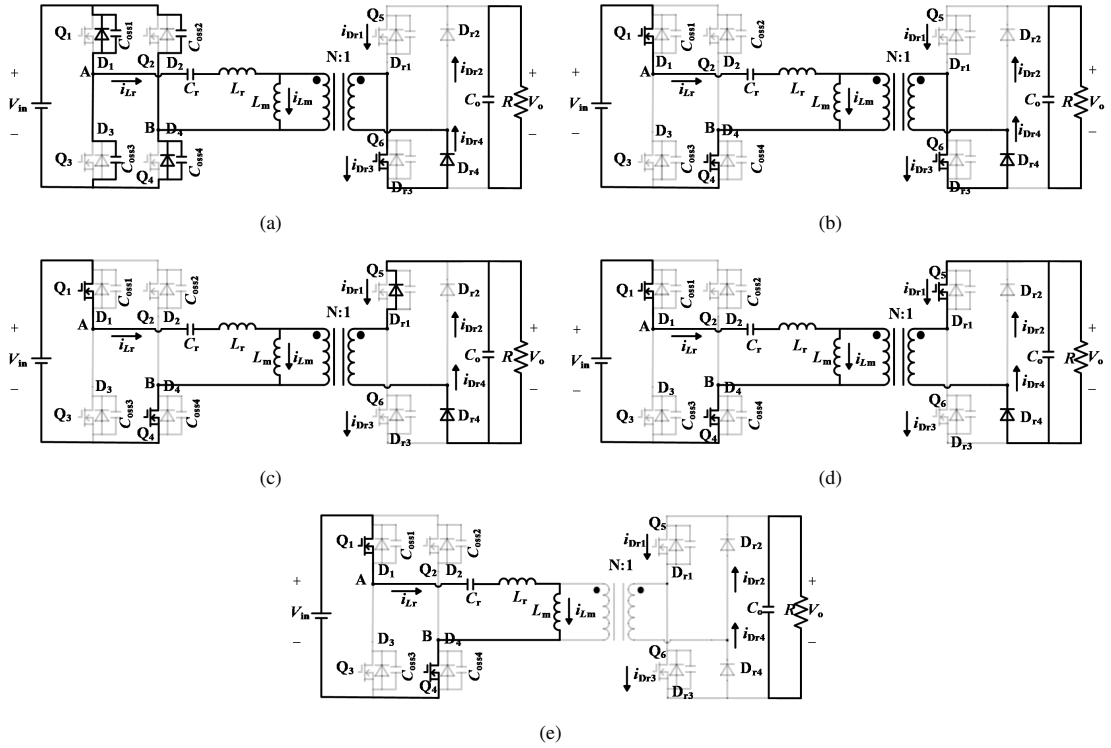

FIGURE 3 Equivalent circuit over half switching period in short-circuit control mode. (a) Mode I [t_0-t_1]. (b) Mode II [t_1-t_2]. (c) Mode III [t_2-t_3]. (d) Mode IV [t_3-t_4]. (e) Mode V [t_4-t_5].

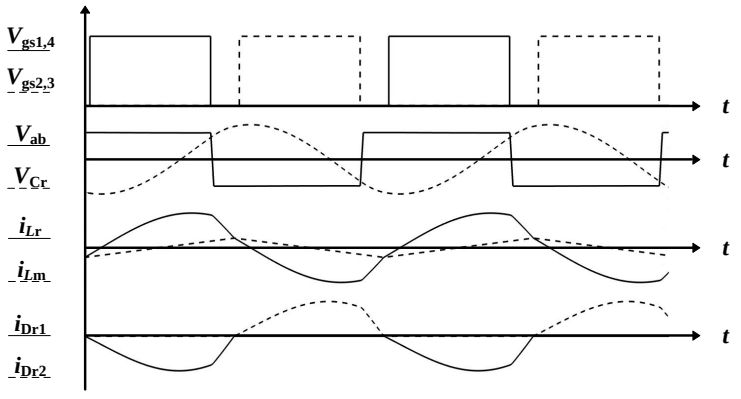

FIGURE 4 Key waveforms of PFM control mode.

The operation of t_5-t_{10} is similar to that of t_0-t_5, so it is not discussed here.

The switching frequency f_s is higher than the resonant frequency f_r in PFM control mode. There is no drive signal on the secondary side, and the output voltage is regulated by adjusting f_s. The proposed converter works in the same way as the *LLC* resonant converter, and the waveforms of key parameters in this mode are shown in Fig. 4.

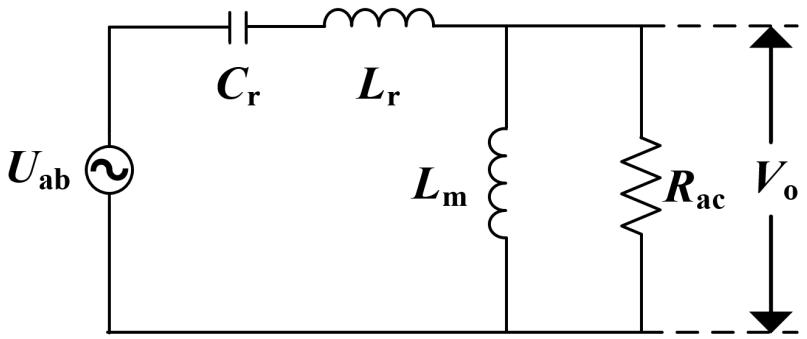

FIGURE 5 Equivalent circuit model of the converter in PFM control mode.

3 | CIRCUIT ANALYSIS

3.1 | Voltage Gain

When the converter operates in PFM control mode, the equivalent circuit model can be simplified as shown in Fig. 5. Where $R_{ac} = 8n^2R/\pi^2$ is the equivalent resistance. According to this equivalent circuit, the voltage gain in PFM control mode can be derived as follows:

$$\begin{aligned} G = \frac{V_o}{V_{in}} = \frac{1}{n}M &= \frac{1}{n}\frac{(sL_m)//R_{ac}}{\frac{1}{sC_r} + sL_r + (sL_m)//R_{ac}} \\ &= \frac{1}{n}\frac{1}{\sqrt{(1+\lambda-\frac{\lambda}{f_n^2})^2 + Q^2\cdot(f_n - \frac{1}{f_n})^2}} \end{aligned} \tag{8}$$

where $\lambda = L_r/L_m$, $f_n = f/f_r$, $Q = \sqrt{L_r/C_r}/R_{ac}$. It should be noted that the voltage gain is inversely proportional to the switching frequency when the switching frequency exceeds the resonant frequency. Hence, the output voltage decreases with the increase of the switching frequency.

During the short-circuit control mode, the voltage applied to the resonant inductor L_r increases due to the short-circuit of the secondary side, which delivers a higher amount of energy to the load. Meanwhile, the current through the diodes on the secondary side is discontinuous. Therefore, the operating process in this mode can be regarded as the Boost circuit in DCM mode. The equivalent circuit and the voltage and current waveforms of the inductor in this mode are shown in Fig. 6. It is assumed that the duty ratio of the switch is D_b, and the inductor current takes xT $(0 < x < 1 - D_b)$ to drop to zero after the switch S is turned off. According to the principle of inductor volt-second balance, the following equation can be obtained:

$$V_{in}D_bT = (nV_o - V_{in})xT \tag{9}$$

The average inductor current can be expressed as:

$$I_{ave} = \frac{V_{in}D_bT}{2L_r} \tag{10}$$

The average output current can be obtained as:

$$I_o = \frac{1}{T}\int_{t_{on}}^{t_2} I_{ave}dt = xI_{ave} \tag{11}$$

It can also be expressed as:

$$I_o = \frac{nV_o}{R_{ac}} \tag{12}$$

From (9)-(12), it follows that:

$$n(\frac{V_o}{V_{in}})^2 - \frac{V_o}{V_{in}} - \frac{R_{ac}{D_b}^2T}{2nL_r} = 0 \tag{13}$$

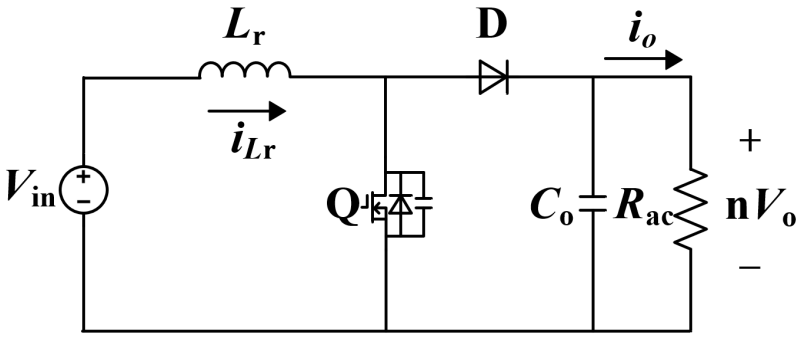

(a)

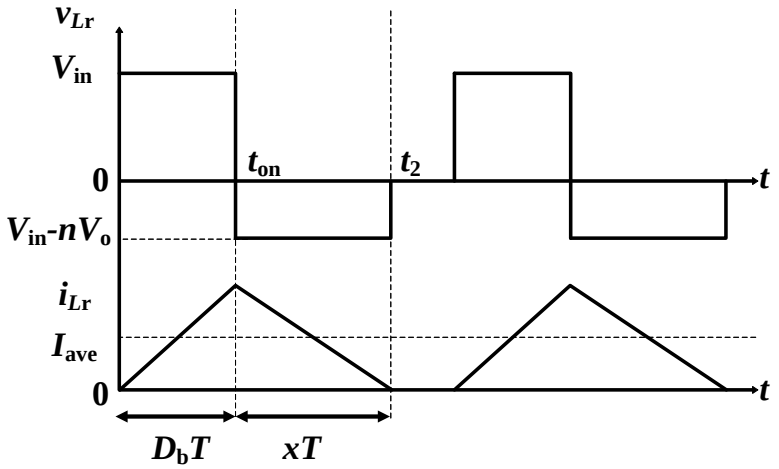

(b)

FIGURE 6 During the short-circuit control mode:(a) The equivalent circuit of the converter. (b) The voltage and current waveforms of the inductor.

Since there are two short-circuit controls in one switching period, the positive solution of the equation can be found by substituting $D_b = 2D$ into the above equation:

$$G = \frac{V_o}{V_{in}} = \frac{1 + \sqrt{1 + \frac{8D^2 T R_{ac}}{L_r}}}{2n} = \frac{1 + \sqrt{1 + \frac{64D^2 n^2 R}{\pi^2 f L_r}}}{2n} \tag{14}$$

As can be observed from the above equation, the voltage gain of the converter is *1/n* when $D = 0$, which is the same as the gain when the converter operates at its resonant frequency in PFM control mode. For a more intuitive analysis of the effect of short-circuit duty cycle D and quality factor Q on voltage gain, the voltage gain can also be expressed as:

$$G = \frac{1 + \sqrt{1 + \frac{16\pi D^2}{Q}}}{2n} \tag{15}$$

Under the condition that the transformer turns ratio remains constant ($n = 1$), the relationship among voltage gain G, short-circuit duty ratio D, and quality factor Q in short-circuit control mode is shown in Fig. 7. As can be seen in Fig. 7, the voltage gain can be improved by increasing D or reducing Q. Nevertheless, increasing D may bring the converter to CCM mode, and decreasing Q can also bring the risk of excessive voltage stress of components. Therefore, the appropriate values of D and Q should be selected with comprehensive consideration.

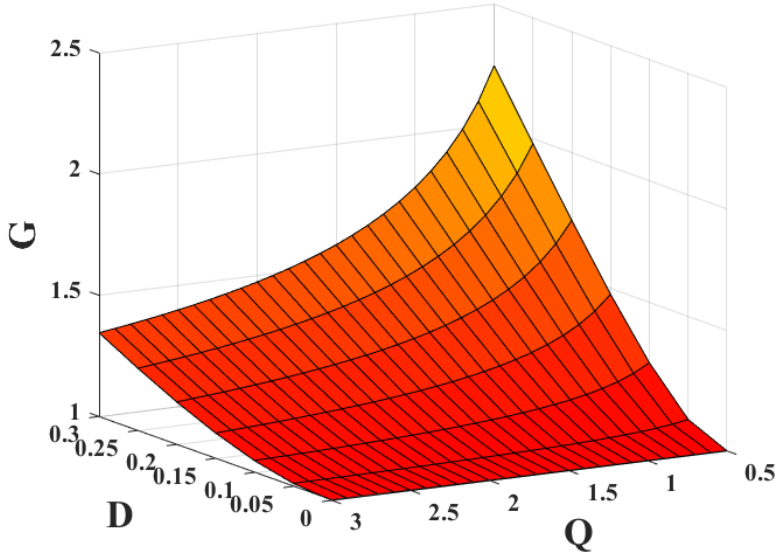

FIGURE 7 Three-dimensional voltage gain G curves versus D and Q (n=1).

3.2 | ZVS Performance

The conditions for the primary-side switches to achieve ZVS in PFM control mode have been analyzed in literature.[22] The converter has to operate in DCM mode to ensure the primary-side switches with ZVS in short-circuit control mode. In literature,[23] an accurate *LLC* model is established by mode analysis. Furthermore, the boundaries and distribution of modes are discussed. Analysis with a similar method is illustrated in the following section.

The converter can operate in three resonant stages (stage P,O,N) depending on the short-circuit duty ratio and load conditions. In the half switching cycle, i.e., Q_1, Q_4 turn ON and Q_2, Q_3 turn OFF, the different resonant stages can be distinguished by the clamping voltage on L_m.

Stage P: The voltage on L_m is clamped to nV_o, $V_{Lm} = nV_o$. Stage O: The voltage on L_m is not clamped, $|v_{Lm}| \leqslant nV_o$. Stage N: The voltage on L_m is clamped to $-nV_o$, $V_{Lm} = -nV_o$. It should be noted that the P and N stages include the case where the L_m voltage is clamped to zero due to the short circuit of the secondary side. In the other half switching cycle when Q_2, Q_3 turn ON and Q_1, Q_4 turn OFF, the definitions of P and N modes are opposite to those mentioned above. The following discussion focuses on the half switching cycle when Q_1, Q_4 turn ON and Q_2, Q_3 turn OFF. Various operation modes of the converter are formed by different sequential combinations of the three stages in a half switching cycle. Fig. 8 shows three operation modes waveforms in short-circuit control mode. As shown in Fig. 8(a), the PO mode starts at t_0 when Q_2, Q_3 turn OFF. i_{Lm} and i_{Lr} have the same negative initial value, and the converter enters stage P. i_{Lm} equals to i_{Lr} at t_4, with a stage switching from P to O. Then, L_m and L_r resonate with C_r, and the voltage on L_m decreases but is always above $-nV_o$ until t_5. Otherwise, the converter will enter stage N within the half switching cycle. Since there is no energy delivery from the primary side to the secondary side in stage O, the current between D_{r2} and D_{r4} is discontinuous. By increasing the load or short-circuit duty ratio D, the converter may change from PO mode to PON mode as shown in Fig. 8(b). The initial values of i_{Lm} and i_{Lr} are different negative values at t_0. The converter switches to stage O from stage P at t_4, while the voltage on L_m decreases below $-nV_o$ before t_5. Thus, the converter moves to stage N, with the short-circuit current flowing through Q_5 on the secondary side. As shown in Fig. 8(c), the PN mode starts at t_0 with a positive initial value of i_{Lr} and a negative initial value of i_{Lm}, which makes the primary-side MOSFETs unable to achieve ZVS. i_{Lr} equals to i_{Lm} at t_4, after which L_m will not resonant with L_r and C_r. The converter enters stage N directly without the appearance of stage O. Meanwhile, the converter operates in CCM with a continuous current on the secondary side.

According to the analysis mentioned above, in order to achieve ZVS of the primary side switches, the converter should operate in PO or PON mode in short-circuit control mode, and avoid working in PN mode. From (1) and (2), v_{Cr} and i_{Lr} at t_2 can be

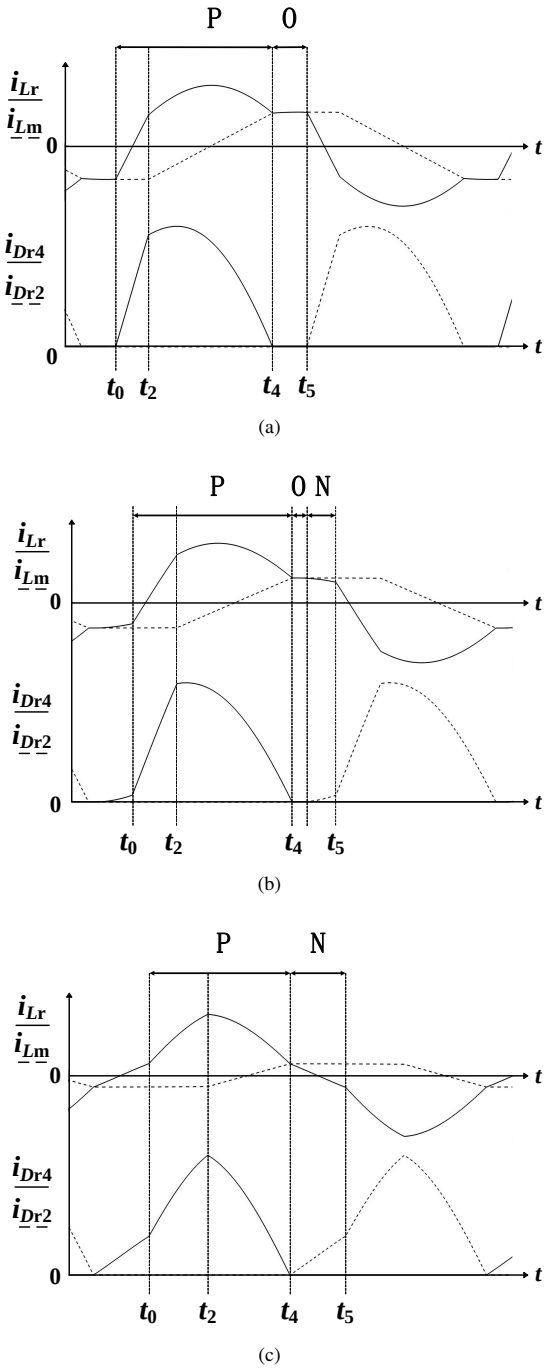

FIGURE 8 Waveforms of different operation modes in short-circuit control mode:(a) PO mode. (b) PON mode. (c) PN mode.

expressed as:

$$\begin{cases} V_{Cr1} = v_{Cr} = V_{in} + (V_{Cr0} - V_{in}) \cos w_r DT + I_{Lr0} Z_r \sin w_r DT \\ I_{Lr1} = i_{Lr} = I_{Lr0} \cos w_r DT + \frac{V_{in} - V_{Cr0}}{Z_r} \sin w_r DT \end{cases} \tag{16}$$

The voltage on L_m is clamped to nV_o in t_2-t_4. Hence,

$$t_4 - t_2 = \frac{2I_{Lr0}}{\frac{nV_o}{L_m}} = \frac{2L_m I_{Lr0}}{nV_o} \tag{17}$$

The boundary condition at the edge of PON mode to PN mode is:

$$L_m \cdot \frac{di_{Lr}}{dt}(t_4) = -nV_o \tag{18}$$

After combining (4) and (16)-(18), we can obtain:

$$-I_{Lr1} \sin \frac{2L_m w_r I_{Lr0}}{nV_o} + \frac{V_{in} - nV_o - V_{Cr1}}{Z_r} \cos \frac{2L_m w_r I_{Lr0}}{nV_o} = \frac{-nV_o}{L_m \cdot w_r} \tag{19}$$

The short-circuit duty cycle that satisfies the above equation is D_0, and in order to avoid the converter entering PN mode, the short-circuit duty cycle in practical operation should not exceed D_0.

The required current for charging and discharging C_{oss1} and C_{oss4} in the dead time can be calculated according to the following equation:

$$I_p = 2C_{oss} \frac{V_{in}}{T_d} \tag{20}$$

where $C_{oss} = C_{oss1} = C_{oss4}$, T_d is the dead time, the resonant current at t_1 when Q_1, Q_4 turn ON can be expressed as:

$$i_{Lr} = I_{Lr0} \cos w_r T_d + \frac{V_{in} - V_{Cr0}}{Z_r} \sin w_r T_d \tag{21}$$

In order to achieve ZVS of the primary-side switches, $i_{Lr} > I_p$ is supposed to be satisfied.

4 | EXPERIMENTAL RESULTS

A 3.3 kW laboratory prototype of the proposed converter, in which all switches are SiC devices, has been built to verify the theoretical analysis above. The components list of the proposed converter is presented in Table 1. Fig. 9 shows the photograph of the experimental prototype. In order to make a comparison with the proposed converter and the conventional *LLC* converter, under the same input and output voltage and load conditions, the modulation method proposed and the traditional *LLC* modulation method are used for experiments, respectively.

TABLE 1 Parameters and components of the prototype

Component	Symbol	Value/Type
Input voltage	V_{in}	400V
Output voltage	V_o	250V-430V
Output power	P_o	3.3kW
Resonant frequency	f_r	98.7kHz
Resonant capacitor	C_r	52nF
Resonant inductor	L_r	50μH
Magnetizing inductor	L_m	100μH
Turns ratio of transformer	n	1.1:1
Transformer core		PQ5050
SiC MOSFETs	Q_{1-6}	UJ3C065030K3S
SiC diodes	$D_{r2,4}$	UJ3D06530

The switching waveforms of Q_1, and the waveforms of i_{Lr} and V_o are shown in Fig. 10. These waveforms are tested under short-circuit control mode at full-load condition, the input voltage is 400V, the switching frequency is equal to the resonant frequency (fr=98.7kHz), and the short-circuit duty ratio D is 0.1. As shown, the output voltage is 430V; the RMS value of resonant current is i_{Lr-RMS}=9.23A; the peak-to-peak value of magnetizing current is ΔI_{Lm}=11.09A; the peak-to-peak value of resonant current is ΔI_{Lr}=29.45A. The experimental waveform is consistent with the simulation, which verifies the theoretical analysis of the topology. When other conditions remain unchanged, the same prototype is used with the traditional *LLC* frequency modulation. Note that the secondary side can be regarded as a full-bridge rectifier without driving signals. The key waveforms at full-load condition with the switching frequency f_s=85kHz and output voltage V_o=430V are illustrated in Fig. 11. As illustrated in Fig.

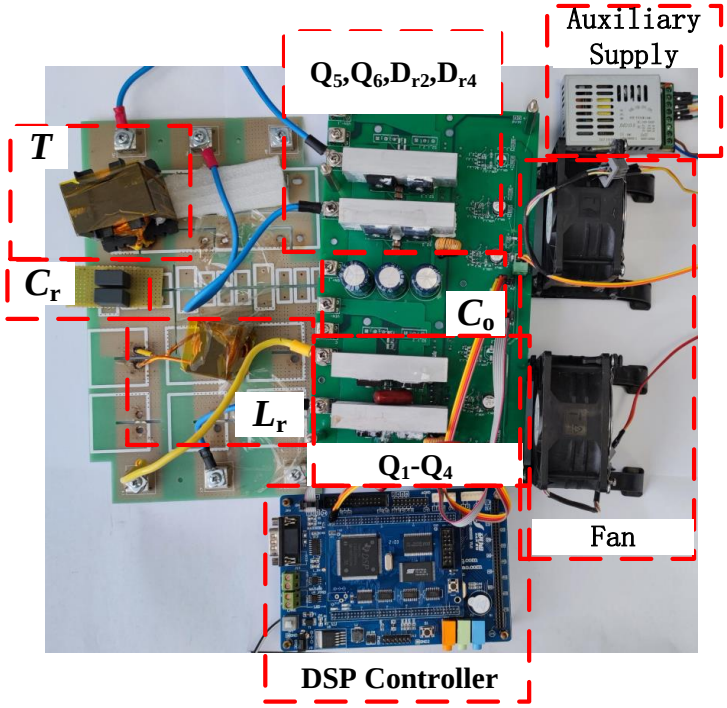

FIGURE 9 Experimental prototype.

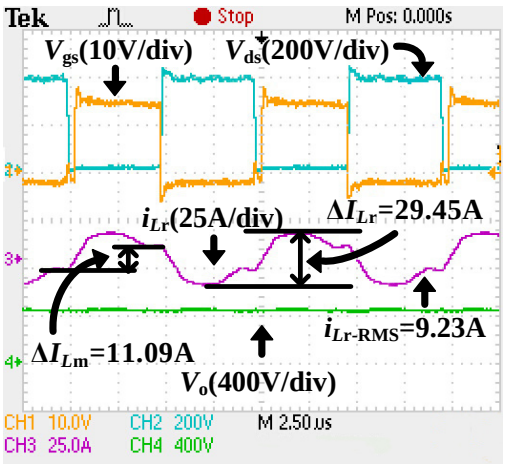

FIGURE 10 Experimental steady-state waveforms under full-load condition with V_{in}=400V, V_o=430V in short-circuit control mode.

11, the RMS value of resonant current is i_{Lr-RMS}=11.9A; the peak-to-peak value of magnetizing current is ΔI_{Lm}=24.95A; the peak-to-peak value of resonant current is ΔI_{Lr}=36.12A. Therefore, the magnetizing current and the resonant current in the traditional *LLC* frequency modulation are higher than those in short-circuit control mode.

In order to compare the efficiency of the converters under different control methods, the efficiency curves of 400V input and 430V output are measured as shown in Fig. 12. As can be seen in Fig. 12, the converter can work with higher efficiency in short-circuit control mode, so the converter proposed in this paper can effectively reduce the resonant current, thus reducing the loss and making the converter more efficient in the whole load range. According to the law of electromagnetic induction, we can get

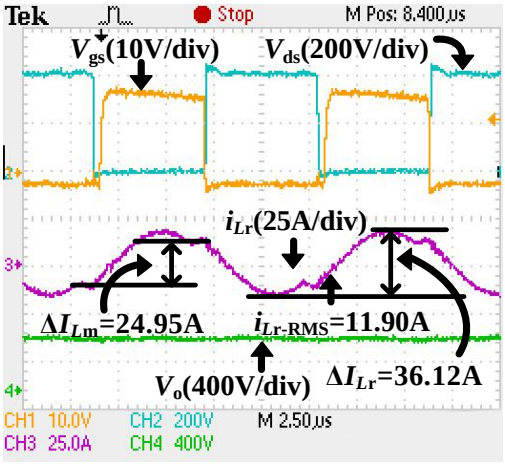

FIGURE 11 Experimental steady-state waveforms under full-load condition with V_{in}=400V, V_o=430V in the traditional *LLC* frequency modulation.

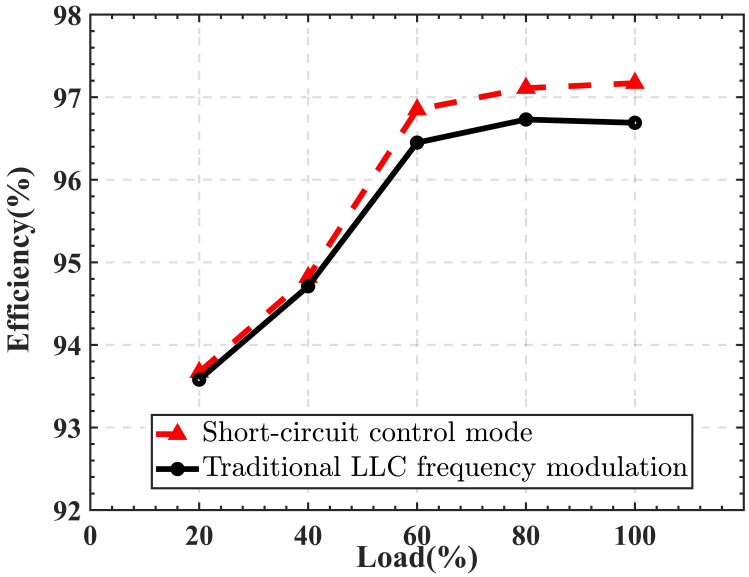

FIGURE 12 Efficiency comparison of different control methods.

the following:

$$L_m i_{Lm-max} = \frac{L_m \Delta I_{Lm}}{2} = N_p A_e B_{max} \tag{22}$$

$$V_p = 4 N_p A_e B_{max} f_{min} = n V_o \tag{23}$$

where B_{max} is the maximum magnetic flux density, i_{Lm-max} is the maximum magnetizing current, N_p is the number of turns of primary winding, A_e is the effective cross-sectional area of magnetic core, and V_p is the primary voltage of transformer. It can be seen that the converter proposed in this paper has smaller ΔI_{Lm} than the traditional *LLC* resonant converter, and the minimum switching frequency f_{min} is equal to the resonant frequency f_r. According to (22) and (23), the proposed converter can minimize the core volume of the transformer, resulting in lower core loss and higher power density.

When the converter works in PFM control mode, the key waveforms at full-load condition with the switching frequency f_s=120kHz and input voltage V_{in}=400V are illustrated in Fig. 13. As can be seen, the primary-side switches achieve ZVS with an output voltage of 250V.

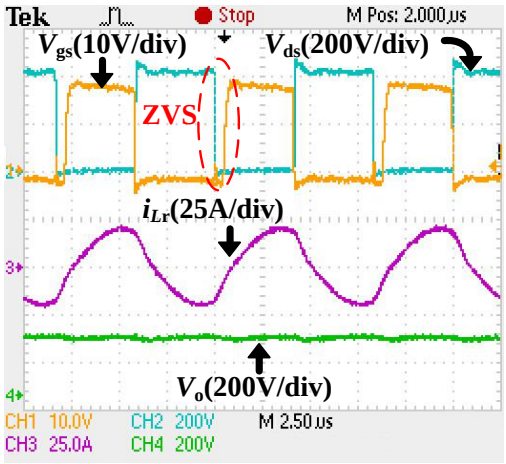

FIGURE 13 Experimental steady-state waveforms under full-load condition with V_{in}=400V, V_o=250V in PFM control mode.

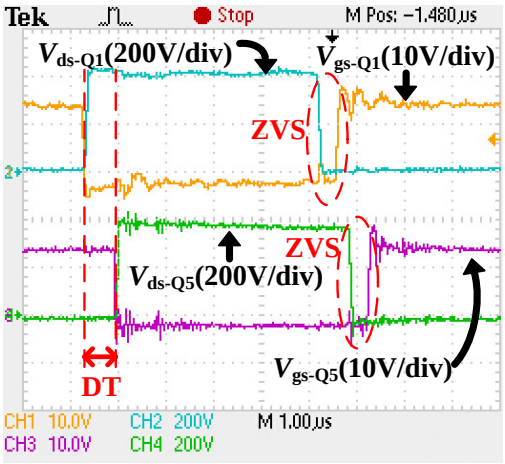

FIGURE 14 Experimental steady-state ZVS waveforms under full-load condition with V_{in}=400V, V_o=430V in short-circuit control mode.

Furthermore, the converter has been tested under the most challenging conditions for the primary-side switches to achieve ZVS in short-circuit control mode with an input voltage of 400V, an output voltage of 430V, and a maximum short-circuit duty ratio of 0.1. Fig. 14 shows gate-source voltage and drain-source voltage of the primary-side switch Q_1 and the secondary-side switch Q_5 under this condition. As shown, Q_5 turns on after Q_1, and the switches achieve ZVS on both sides.

To verify the calculated gain by experiments and simulations, Fig. 15 shows the gains obtained by calculations, experiments, and simulations according to the corresponding short-circuit duty ratios at full-load condition. It can be observed that the simulated values are basically the same as the calculated values when the short-circuit duty cycle is less than 10%, while the converter gradually enters the CCM after the short-circuit duty cycle exceeds 10%, and the equation proposed above is no longer suitable. The gain observed in the experiment is lower than the others because the calculation and simulation are performed under ideal conditions and the voltage drops between wires and switching devices are ignored. Fig. 16 shows the efficiency curves of the experimental prototype under 400V input, different output voltages and loads. As shown, the peak efficiency of the experimental prototype reaches 97.25%, and the working efficiency of the converter is higher than 96% when the load is above 60%.As the output power of the proposed converter increases, it can be seen from (22) that the magnetic flux density in the transformer and

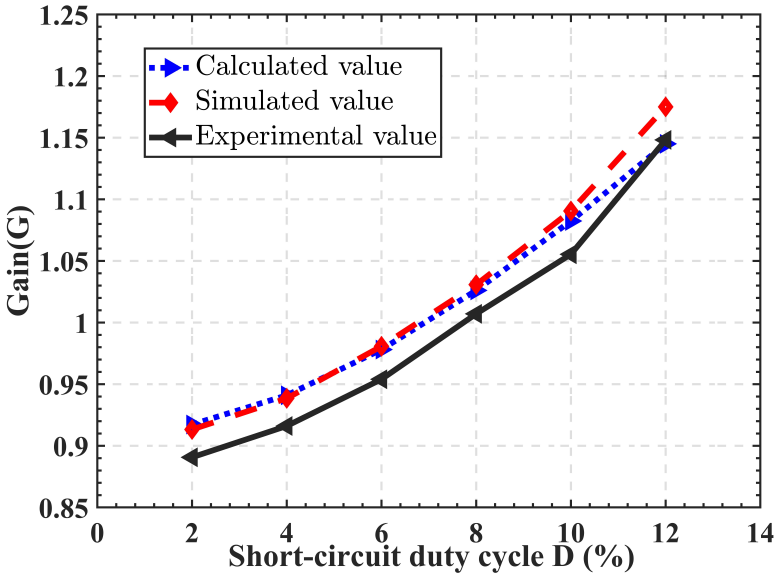

FIGURE 15 The voltage gains obtained by calculations, experiments, and simulations according to the corresponding short-circuit duty ratios at full-load condition.

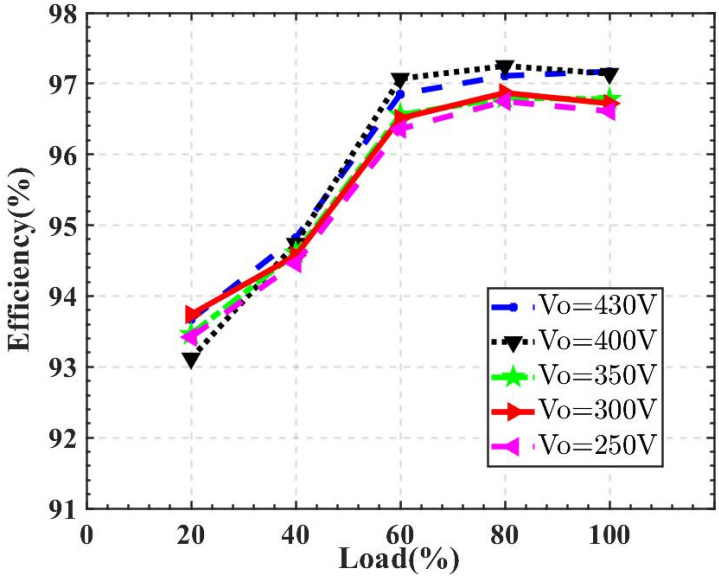

FIGURE 16 Efficiency curves of the experimental prototype under 400V input, different output voltages and loads.

resonant inductor increases, and the core loss of magnetic components increases according to the Steinmetz equation. Meanwhile, the increase of resonant current will bring more copper loss and conduction loss of switches. Therefore, the efficiency will decrease when the load is above 80%.

Table 2 shows the comprehensive comparison between the proposed converter and some state-of-the-art topologies with wide output voltage range. As can be seen, many topologies have been proposed to improve the performance of *LLC* for wide output voltage range applications. In literature,[24] a resonant converter with notch resonant tank is proposed, the converter features narrow switching frequency and great soft-switching performance. However, the additional *LC* resonant tank brings higher core loss and increases the current stress on the primary side. To improve the performance in wide output voltage range applications,

TABLE 2 Comparison with the state-of-the-art wide output voltage range topologies

Topologies	[24]	[25]	[26]	[27]	[28]	This work
Modulation	PFM	PWM	PFM	PWM	PWM	PSM
Number of switches	4	5	4	6	5	6
Number of diodes	4	6	4	6	3	2
Number of transformers	1	1	2	2	1	1
Number of resonant inductors	2	1	2	2	1	1
Number of filter capacitors	1	2	4	2	2	1
Input voltage	380V	390V	400V	390V	390V	400V
Output voltage	50V-430V	250V-420V	50V-420V	230V-440V	250V-420V	250V-430V
Output power	3kW	1.3kW	1.5kW	1.3kW	1kW	3.3kW
Peak efficiency	96.8%	93.94%	95.65%	97.31%	96.7%	97.25%

the secondary-side structure of *LLC* is modified in literature[25,26], and interleaving structure is introduced in literature[27,28]. However, the introduction of extra components leads to additional power loss and costs and degrades the power density. In literature,[26] a modified voltage doubler architecture consisting of three diodes and a PWM-controlled auxiliary switch on the secondary side is proposed to improve the output voltage range and power density. However, there are oscillations in the voltage and current of the auxiliary switch. Compared with the literature, the proposed converter can achieve high efficiency with a small number of components, which makes it a competitive candidate for OBC applications.

5 | CONCLUSION

In this paper, a resonant converter with hybrid modulation is proposed to realize wide-range output voltage with high efficiency for OBC applications. Voltage gain modulation is realized by adjusting the switching frequency or the short-circuit duty cycle depending on the required voltage gain. The proposed topology demonstrates benefits that include the following:

1. Simple topology and control method. Compared with the traditional *LLC* topology, only two diodes are replaced by MOSFETs on the secondary side, and no auxiliary components are added.
2. Excellent soft-switching performance. In short-circuit control mode, all switches can achieve ZVS, and the secondary-side diodes can achieve ZCS. Primary-side switches are able to achieve ZVS in PFM control mode.
3. Wide voltage regulation range. A wide output voltage range can be achieved in a narrow switching frequency.
4. Energy delivery with high power density and high efficiency. The proposed converter can effectively reduce the RMS value and the peak-to-peak value of resonant current, and reduce the volume of transformer core. Therefore, power density and efficiency are improved.

Finally, a 3.3 kW experimental prototype with 400V input and 250V-430V output is built to verify the theoretical analysis with the highest efficiency of 97.25%.

References

1. Assadi SA, Matsumoto H, Moshirvaziri M, Nasr M, Zaman MS, Trescases O. Active Saturation Mitigation in High-Density Dual-Active-Bridge DC–DC Converter for On-Board EV Charger Applications. *IEEE Transactions on Power Electronics* 2020; 35(4): 4376-4387. doi: 10.1109/TPEL.2019.2939301
2. Khaligh A, D'Antonio M. Global Trends in High-Power On-Board Chargers for Electric Vehicles. *IEEE Transactions on Vehicular Technology* 2019; 68(4): 3306-3324. doi: 10.1109/TVT.2019.2897050

3. Shen Y, Zhao W, Chen Z, Cai C. Full-Bridge LLC Resonant Converter With Series-Parallel Connected Transformers for Electric Vehicle On-Board Charger. *IEEE Access* 2018; 6: 13490-13500. doi: 10.1109/ACCESS.2018.2811760

4. Zhao H, Shen Y, Ying W, Ghosh SS, Ahmed MR, Long T. A Single- and Three-Phase Grid Compatible Converter for Electric Vehicle On-Board Chargers. *IEEE Transactions on Power Electronics* 2020; 35(7): 7545-7562. doi: 10.1109/TPEL.2019.2956653

5. Wadi A, Abdel-Hafez MF, Hussein AA, Alkhawaja F. Alleviating Dynamic Model Uncertainty Effects for Improved Battery SOC Estimation of EVs in Highly Dynamic Environments. *IEEE Transactions on Vehicular Technology* 2021; 70(7): 6554-6566. doi: 10.1109/TVT.2021.3085006

6. Hua CC, Fang YH, Lin CW. LLC resonant converter for electric vehicle battery chargers. *IET Power Electronics* 2016; 9(12): 2369-2376. doi: https://doi.org/10.1049/iet-pel.2016.0066

7. Deng J, Li S, Hu S, Mi CC, Ma R. Design Methodology of LLC Resonant Converters for Electric Vehicle Battery Chargers. *IEEE Transactions on Vehicular Technology* 2014; 63(4): 1581-1592. doi: 10.1109/TVT.2013.2287379

8. Khaligh A, Dusmez S. Comprehensive Topological Analysis of Conductive and Inductive Charging Solutions for Plug-In Electric Vehicles. *IEEE Transactions on Vehicular Technology* 2012; 61(8): 3475-3489. doi: 10.1109/TVT.2012.2213104

9. Baek J, Kim KW, Youn HS, Kim CE. High-Efficiency LLC Resonant Converter With Reconfigurable Voltage Multiplying Rectifier for Wide Output Voltage Applications. *IEEE Transactions on Power Electronics* 2021; 36(7): 7641-7651. doi: 10.1109/TPEL.2020.3047005

10. Qin J, Moussaoui Z, Liu J, Miller G. Light load efficiency enhancement of a LLC resonant converter. In: 2011 Twenty-Sixth Annual IEEE Applied Power Electronics Conference and Exposition (APEC). ; 2011: 1764-1768

11. Zhao S, Xu J, Trescases O. Burst-Mode Resonant LLC Converter for an LED Luminaire With Integrated Visible Light Communication for Smart Buildings. *IEEE Transactions on Power Electronics* 2014; 29(8): 4392-4402. doi: 10.1109/TPEL.2013.2286104

12. Feng W, Lee FC, Mattavelli P. Optimal Trajectory Control of Burst Mode for LLC Resonant Converter. *IEEE Transactions on Power Electronics* 2013; 28(1): 457-466. doi: 10.1109/TPEL.2012.2200110

13. Shafiei N, Ordonez M, Craciun M, Botting C, Edington M. Burst Mode Elimination in High-Power LLC Resonant Battery Charger for Electric Vehicles. *IEEE Transactions on Power Electronics* 2016; 31(2): 1173-1188. doi: 10.1109/TPEL.2015.2420573

14. Kim BC, Park KB, Moon GW. Asymmetric PWM Control Scheme During Hold-Up Time for LLC Resonant Converter. *IEEE Transactions on Industrial Electronics* 2012; 59(7): 2992-2997. doi: 10.1109/TIE.2011.2166237

15. Liu W, Wang B, Yao W, Lu Z, Xu X. Steady-state analysis of the phase shift modulated LLC resonant converter. In: 2016 IEEE Energy Conversion Congress and Exposition (ECCE). ; 2016: 1-5

16. Zhao Q, Liu W, Wang Y, Wang D, Wu N. A Novel Multiresonant DC–DC Converter With Wide Output-Voltage Range. *IEEE Transactions on Power Electronics* 2020; 35(6): 5625-5638. doi: 10.1109/TPEL.2019.2948217

17. Wang Y, Qi N, Guan Y, Cecati C, Xu D. A Single-Stage LED Driver Based on SEPIC and LLC Circuits. *IEEE Transactions on Industrial Electronics* 2017; 64(7): 5766-5776. doi: 10.1109/TIE.2016.2613921

18. Ta LAD, Dao ND, Lee DC. High-Efficiency Hybrid LLC Resonant Converter for On-Board Chargers of Plug-In Electric Vehicles. *IEEE Transactions on Power Electronics* 2020; 35(8): 8324-8334. doi: 10.1109/TPEL.2020.2968084

19. Zhou J, Ma H. A New LLC Converter with Wide Output Voltage Range and Improved Efficiency at Medium or Low Output Voltage. In: 2019 IEEE 28th International Symposium on Industrial Electronics (ISIE). ; 2019: 734-739

20. Wu H, Li Y, Xing Y. LLC Resonant Converter With Semiactive Variable-Structure Rectifier (SA-VSR) for Wide Output Voltage Range Application. *IEEE Transactions on Power Electronics* 2016; 31(5): 3389-3394. doi: 10.1109/TPEL.2015.2499306

21. Jang Y, Jovanović MM, Ruiz JM, Kumar M, Liu G. Implementation of 3.3-kW GaN-based DC-DC converter for EV on-board charger with series-resonant converter that employs combination of variable-frequency and delay-time control. In: 2016 IEEE Applied Power Electronics Conference and Exposition (APEC). ; 2016: 1292-1299

22. Li B, Zhang X, Zhou D, Sun S, Wang Y, Xu D. Soft-switching Characteristics Analysis Based on LLC Resonant Converter. In: 2018 IEEE Transportation Electrification Conference and Expo, Asia-Pacific (ITEC Asia-Pacific). ; 2018: 1-6

23. Fang X, Hu H, Shen ZJ, Batarseh I. Operation Mode Analysis and Peak Gain Approximation of the LLC Resonant Converter. *IEEE Transactions on Power Electronics* 2012; 27(4): 1985-1995. doi: 10.1109/TPEL.2011.2168545

24. Kim M, Jeong H, Han B, Choi S. New Parallel Loaded Resonant Converter With Wide Output Voltage Range. *IEEE Transactions on Power Electronics* 2018; 33(4): 3106-3114. doi: 10.1109/TPEL.2017.2706360

25. Shang M, Wang H. A Voltage Quadrupler Rectifier Based Pulsewidth Modulated LLC Converter With Wide Output Range. *IEEE Transactions on Industry Applications* 2018; 54(6): 6159-6168. doi: 10.1109/TIA.2018.2850033

26. Wang H, Li Z. A PWM LLC Type Resonant Converter Adapted to Wide Output Range in PEV Charging Applications. *IEEE Transactions on Power Electronics* 2018; 33(5): 3791-3801. doi: 10.1109/TPEL.2017.2713815

27. Shahzad MI, Iqbal S, Taib S. Interleaved LLC Converter With Cascaded Voltage-Doubler Rectifiers for Deeply Depleted PEV Battery Charging. *IEEE Transactions on Transportation Electrification* 2018; 4(1): 89-98. doi: 10.1109/TTE.2017.2753407

28. Li Z, Xue B, Wang H. An Interleaved Secondary-Side Modulated LLC Resonant Converter for Wide Output Range Applications. *IEEE Transactions on Industrial Electronics* 2020; 67(2): 1124-1135. doi: 10.1109/TIE.2019.2897507